

Published in final edited form as:

Nature. 2006 May 25; 441(7092): 523–527.

Identification of a tumour suppressor network opposing nuclear Akt function

Lloyd C. Trotman^{1,2}, Andrea Alimonti^{1,2}, Pier Paolo Scaglioni^{1,3}, Jason A. Koutcher⁴, Carlos Cordon-Cardo², and Pier Paolo Pandolfi^{1,2}

¹ Cancer Biology and Genetics Program, Memorial Sloan-Kettering Cancer Center, Sloan-Kettering Institute, 1275 York Avenue, New York, New York 10021, USA.

² Department of Pathology, Memorial Sloan-Kettering Cancer Center, Sloan-Kettering Institute, 1275 York Avenue, New York, New York 10021, USA.

³ Department of Medicine, Memorial Sloan-Kettering Cancer Center, Sloan-Kettering Institute, 1275 York Avenue, New York, New York 10021, USA.

⁴ Departments of Medicine, Radiology and Medical Physics, Memorial Sloan-Kettering Cancer Center, Sloan-Kettering Institute, 1275 York Avenue, New York, New York 10021, USA.

Abstract

The proto-oncogene AKT (also known as PKB) is activated in many human cancers, mostly owing to loss of the *PTEN* tumour suppressor¹. In such tumours, AKT becomes enriched at cell membranes where it is activated by phosphorylation. Yet many targets inhibited by phosphorylated AKT (for example, the FOXO transcription factors) are nuclear; it has remained unclear how relevant nuclear phosphorylated AKT (pAKT) function is for tumorigenesis. Here we show that the PML tumour suppressor prevents cancer by inactivating pAKT inside the nucleus. We find in a mouse model that *Pml* loss markedly accelerates tumour onset, incidence and progression in *Pten*-heterozygous mutants, and leads to female sterility with features that recapitulate the phenotype of *Foxo3a* knockout mice². We show that *Pml* deficiency on its own leads to tumorigenesis in the prostate, a tissue that is exquisitely sensitive to pAkt levels, and demonstrate that Pml specifically recruits the Akt phosphatase PP2a as well as pAkt into Pml nuclear bodies. Notably, we find that *Pml*-null cells are impaired in PP2a phosphatase activity towards Akt, and thus accumulate nuclear pAkt. As a consequence, the progressive reduction in *Pml* dose leads to inactivation of Foxo3a-mediated transcription of proapoptotic *Bim* and the cell cycle inhibitor *p27^{kip1}*. Our results demonstrate that Pml orchestrates a nuclear tumour suppressor network for inactivation of nuclear pAkt, and thus highlight the importance of AKT compartmentalization in human cancer pathogenesis and treatment.

Pml nuclear bodies represent distinct yet dynamic intranuclear structures involved in apoptosis, proliferation and senescence³. Nuclear bodies are absent from *Pml*-deficient cells, causing aberrant nuclear patterns of nuclear body resident proteins. We have recently reported the high correlation between reduction in nuclear body number and prostate and colon cancer⁴, both tumours showing frequent *PTEN* loss^{5,6}. Because we and others have established faithful mouse models for the role of *PTEN* in cancer^{7–9}, we sought to determine whether *Pml* loss would affect the signature of *Pten* deficiency. After crossing *Pten*-heterozygous mice

Author Information Reprints and permissions information is available at npg.nature.com/reprintsandpermissions. The authors declare no competing financial interests. Correspondence and requests for materials should be addressed to P.P.P. (p-pandolfi@ski.mskcc.org). Supplementary Information is linked to the online version of the paper at www.nature.com/nature.

Author Contributions The experiments were conceived and designed by L.C.T., A.A., P.P.S., J.A.K., C.C.-C. and P.P.P. Experiments were performed by L.C.T., A.A., P.P.S. and J.A.K. Data were analysed by L.C.T., A.A., P.P.S., J.A.K., C.C.-C. and P.P.P. The paper was written by L.C.T. and P.P.P.

(*Pten*^{+/-}) with *Pml*-null mice (*Pml*^{-/-}) to produce six genotypes of interest, we found a marked *Pml*-dependent reduction in lifespan of *Pten*^{+/-} mice (Supplementary Fig. S1a). *Pten*^{+/-} female lethality, dictated by an autoimmune disorder¹⁰, was not precipitated by *Pml* loss. In contrast, the male cohort displayed an exquisite, *Pml* dose dependence in survival (the autoimmune disorder is minor in males¹⁰), thus exposing a novel lethal phenotype in compound mutants with *Pml* haploinsufficiency for its repression. Magnetic resonance imaging (MRI) visualized intestinal and prostate anomalies (not shown), and post-mortem analysis confirmed large intestinal lesions in *Pten*^{+/-}*Pml*^{+/-} and *Pten*^{+/-}*Pml*^{-/-} mice, suggesting obstruction as a probable (males) or additional (females) cause of death. Intestines of *Pten*^{+/-}*Pml*^{-/-} mice presented invasive adenocarcinoma of the colon (Fig. 1a, colon), whereas *Pten*^{+/-} mice displayed only pre-cancerous polyps (Supplementary Fig. S1b, colon). Disease-free survival analysis summarizes onset of the *Pten*^{+/-}*Pml*^{-/-}-specific colon carcinoma (Fig. 1b). Notably, *Pml* levels also dictated polyp numbers in *Pten*^{+/-} animals: *Pml* dose reduction resulted in a 3–5-fold increase in the number of polyps per mouse (Fig. 1b, top inset). Average polyp diameter also correlated with *Pml* status (Fig. 1b, bottom inset). Taken together, in *Pten*^{+/-} mice, *Pml* loss causes the appearance of polyposis and colon cancer, which reduces lifespan severely.

Pten activity regulates prostate cancer, as by 8 months some *Pten*^{+/-} animals develop prostatic intraepithelial neoplasia (the *in situ* form of prostate cancer). Invasive cancer is observed on further lowering of *Pten* activity, as shown in *Pten*-hypomorphic or prostate-specific null mice^{11,12}. Haematoxylin and eosin staining and prostate cancer-free survival analysis revealed that *Pten*^{+/-}*Pml*^{-/-} and *Pten*^{+/-}*Pml*^{+/-} males (but not *Pten*^{+/-} mice) developed highly invasive cancers, suggesting that prostate epithelia are more sensitive to *Pml* status than intestine (Fig. 1 and Supplementary Fig. S1b, prostate). We also found a characteristic increased cell proliferation marker staining¹³ (even in tumour-free areas) in *Pten*^{+/-}*Pml*^{+/-} and *Pten*^{+/-}*Pml*^{-/-} intestines as well as in *Pten*^{+/-}*Pml*^{-/-} prostate glands (Supplementary Fig. S1c).

The degree of *Pten* deficiency closely correlates with activation of the oncogenic kinase Akt¹¹. Akt activation by membrane recruitment is inhibited by Pten^{14,15} and leads to phosphorylation of Akt at Thr 308 and Ser 473 (refs 16, 17). To address whether *Pml* loss affects Akt activation we performed immunohistochemistry (IHC) staining and quantified western blotting of tissues. Staining of pAkt at Ser 473 was clearly increased in polyps, normal colon and in prostate lesions of *Pten*^{+/-}*Pml*^{-/-} mice when compared with *Pten*^{+/-} mice (Fig. 2a). Importantly, both colon and prostate presented dominant nuclear pAkt accumulation, indicating a qualitative change in kinase localization (Fig. 2a, insets). Quantification of pAkt levels in *Pten*^{+/-} mice confirmed a 50% increase in normal colon and 2-month-old prostate on *Pml* loss (Supplementary Fig. S1d, compare *Pten*^{+/-}*Pml*^{-/-} (en) and *Pten*^{+/-}*Pml*^{+/-} (ew)), comparable to the reported *Pten*^{+/+} to *Pten*^{+/-} transition¹¹. Loss of the remaining *Pten* allele was excluded through western blot (not shown), IHC and Southern blot analysis of the macro-dissected cancers (Supplementary Fig. S1e). Taken together, our data suggest that in *Pten*^{+/-} mice, loss of *Pml* leads to further activation of Akt but not because of complete *Pten* loss.

When analysing *Pten*^{+/+} prostates we found that *Pml*^{-/-} animals presented high-grade prostatic intraepithelial neoplasia and areas of focally invasive cancer in their anterior prostates around 12 months of age (Fig. 2b and Supplementary Fig. S2a, b). Normal colon and prostate in *Pml*-deficient mice showed increased levels of pAkt (Fig. 2c) but no signs of colon neoplasia/dysplasia, consistent with the above finding that prostate is most sensitive to *Pml* loss (Fig. 1b). We frequently found enlarged prostates in *Pml*-null mice, yet larger organ size was also due to large luminal non-cellular areas (see Supplementary Fig. S2c, asterisk in the *Pten*^{+/-}*Pml*^{+/+} panel). To measure size effects we determined average individual cell (not organ) sizes. *Pml*^{-/-} and *Pten*^{+/-} glands were mostly hypercellular but filled with cells of only

half the size of their wild-type counterparts (Supplementary Fig. S2c). Thus, *Pml* deficiency leads to Akt activation in prostate and colon and triggers initiation of prostate cancer.

To test whether the qualitative difference in pAkt localization was an inherent feature of *Pml* loss we used mouse embryonic fibroblasts (MEFs). First, we determined Akt status in primary littermate *Pml*^{+/+} and *Pml*^{-/-} MEFs by subjecting them to serum starvation and stimulation (see Methods). These cells had little and comparable pAkt activation at steady state and during serum starvation (Supplementary Fig. S2d, top panels). But serum stimulation for 10 min gave stronger Akt activation in *Pml*^{-/-} than in *Pml*^{+/+} MEFs, as confirmed by Akt kinase assays (Supplementary Fig. S2e). At 3 h after stimulation, Akt activation was slightly higher in null MEFs, an effect more readily observed at later passage (Supplementary Fig. S2f, top panels). To test whether transgenic expression of human *PML* also affects Akt activation we used stably *PML*-transduced *Pml*^{-/-} cells, which showed decreased Akt activation and faster inactivation after stimulation (Supplementary Fig. S2d, bottom panels). *PML* over-expression in *Pml*^{+/+} MEFs had almost no effect (not shown), similar to overexpression in *PML*^{+/+} human cells (Supplementary Fig. S2f, middle panels). Thus, *Pml* is able to suppress Akt activation after a membrane stimulus and it is sufficient to remedy this defect in *Pml*^{-/-} cells. To exclude effects on Akt caused by cell cycle perturbations after *PML* add back, cell cycle profiles of *Pml*^{-/-} and add-back cells were compared but no differences found, especially after starvation/stimulation (Supplementary Fig. S2g).

To account for qualitative and quantitative differences by confocal laser scanning microscopy (CLSM), primary *Pml*^{+/+} and *Pml*^{-/-} MEFs were seeded on the same coverslips. Minor differences in pAkt staining were observed between wild-type and null cells at steady state and starvation (Fig. 3a). In contrast, *Pml*^{-/-} cells showed not only stronger but notably nuclear pAkt accumulation after 10 min or 3 h of serum stimulation (see also Supplementary Fig. S3a). This localization was in marked contrast to that observed in *Pten*^{-/-} cells, where pAkt is concentrated at cell membranes (Fig. 3a, bottom row). This membrane-associated pAkt pool was not antagonized by overexpression of *PML* in these MEFs (not shown), or in human *PTEN*^{-/-} cells (Supplementary Fig. S2f, bottom panels), consistent with inhibition of nuclear, not cytoplasmic, pAkt by *PML*. Cell fractionation confirmed that a distinct nuclear population of pAkt was present in *Pml*^{-/-} but not *Pml*^{+/+} cells after stimulation (Supplementary Fig. S3b). We next compared pAkt localization in three invasive prostate cancer models. The prostate-specific *Pten*-null and *Pten*-hypomorphic models showed strong membrane accumulation of pAkt, as previously described¹¹ (Fig. 3b). In contrast, the invasive prostate cancer of *Pten*^{+/-} *Pml*^{-/-} mice showed dominant nuclear and cytoplasmic staining (see also Fig. 2a, insets). Therefore, we next tested whether *Pml* loss would enhance nuclear pAkt function.

The forkhead transcription factor FOXO3A is a well-studied nuclear target of pAKT¹⁸, as AKT-mediated phosphorylation causes FOXO3A inactivation and export¹⁹. We quantified nuclear Foxo3a amounts by western blotting and found that *Pml*^{-/-} cells, in contrast to wild-type cells, had decreased exogenous and endogenous nuclear Foxo3a after serum stimulation (Supplementary Fig. S3c). To quantify Foxo3a distribution by non-disruptive means, GFP-FOXO3A (human FOXO3A tagged with green fluorescent protein) localization in fixed *Pml*^{+/+} and *Pml*^{-/-} MEFs was scored. At 10 min after stimulation, 80% of *Pml*^{-/-} cells showed cytoplasmic FOXO3A whereas 70% of wild-type cells still retained FOXO3A in the nucleus (Supplementary Fig. S3d). Importantly, an Akt-insensitive FOXO3A mutant retained its nuclear localization even after a 3 h stimulation in *Pml*^{-/-} cells. In agreement, a twofold increase in Akt-mediated FOXO3A phosphorylation was observed after serum stimulation when comparing *Pml*-deficient cells with add-back cells (Supplementary Fig. S3e).

Foxo3a exerts some of its tumour-suppressive functions by inducing transcription of *p27^{kip1}* (see ref. 18), which inhibits prostate cancer after *Pten* loss¹³. As quantified by real-time

polymerase chain reaction (PCR), *Pml* status effectively dictates *p27^{kip1}* messenger RNA levels in prostates of both *Pten^{+/+}* and *Pten^{+/-}* mice (Fig. 3c). Two additional Foxo3a target genes—the proapoptotic factor Bim and DNA repair protein Gadd45 (ref. 18)—responded similarly, consistent with Foxo3a inactivation (see also Supplementary Fig. S3f).

Foxo3a-deficient females display early infertility due to premature ovarian failure^{20,21}, an event normally associated with ageing². To determine the effect of *Pml* loss on fertility we set up mating pairs using fertile wild-type males. *Pml^{-/-}* and *Pten^{+/-}* females accumulated litters (Supplementary Fig. S4a) similar to wild-type mice (not shown). In contrast, although *Pten^{+/-}Pml^{-/-}* females had near-normal first litter sizes, they were invariably infertile by 5 months of age and their ovaries showed signs of follicular degeneration at 2 months and near-complete follicle depletion by 5 months (Supplementary Fig. S4b). Taken together, our results demonstrate that *Pml* loss enhances Foxo3a inactivation, especially under conditions of elevated Akt (*Pten* loss *in vivo*, serum stimulation *in vitro*).

Mechanistically, *Pml* loss could either stimulate Akt activation or antagonize pAkt inactivation. To distinguish between the two, we used okadaic acid, which selectively inactivates PP2a, the only known Akt-Thr 308 phosphatase^{22,23}. If *Pml* deficiency favours Akt activation mechanisms (independent of PP2a), okadaic acid treatment should increase Akt phosphorylation at Thr 308 in *Pml^{-/-}* cells. Alternatively, if *Pml* deficiency antagonizes PP2a, *Pml^{-/-}* cells should be insensitive to okadaic acid. Our results suggest the latter: *Pml^{-/-}* MEFs, in contrast to wild type, showed no response in the levels of pAkt at Thr 308 on okadaic acid addition in fresh serum (Fig. 4a and Supplementary Fig. S4c). Thus, after this stimulation in the presence of okadaic acid, *Pml^{+/+}* cells were finally able to match the pAkt levels of *Pml^{-/-}* cells (Fig. 4b). Importantly, *Pml^{-/-}* cell extracts retained normal PP2a levels and general activity, suggesting that Pml specifically cooperates with PP2a in pAkt inactivation (Supplementary Fig. S4d, e).

PP2a is a heterotrimer of A, B and catalytic (C) subunits, which can function alone or in a ‘core dimer’ with A. Whereas the two known A and C subunit isoforms are ubiquitous, the B subunit families can determine tissue/substrate specificity and give rise to over 70 holoenzyme variations²⁴. We found the C and to some extent the A subunits co-precipitating with Pml (Fig. 4c), which prompted us to test whether PP2a could act in nuclear bodies. Co-immunoprecipitation experiments showed that Akt is able to associate with Pml both when activated or not (Fig. 4d); using CLSM of primary MEFs, significant nuclear body co-localization of PP2a-C and PP2a-A with Pml as well as nuclear body enrichment was evident (Fig. 4e), and PP2a-C was also found enriched in many *Pml^{+/+}* (but not *Pml^{-/-}*) nuclei (Supplementary Fig. S4f). No Pml co-localization was found in the randomly tested PP2a-B PR-55 family members (Supplementary Fig. S4g).

As a result of probing PML deletion mutants for their ability to bind endogenous PP2a-C, we found that deletion of the RBCC motif abolished binding whereas the RING finger motif was dispensable (Fig. 4f), thus delineating the necessary interaction domains (Supplementary Fig. S5a). Similarly, Δ RBCC was unable to antagonize pAkt activation (Supplementary Fig. S5b). PP2a might also affect Akt indirectly via PDK1 (ref. 25), but we found unaltered steady-state phosphorylated PDK1 levels in tissues and MEFs of various genotypes (not shown) and similar steady-state levels of pAkt in *Pml^{+/+}* and *Pml^{-/-}* cells (Supplementary Figs S3b, cytoplasm, and S5c, nucleus). Specific enrichment of pAkt in Pml nuclear bodies was found in wild-type MEFs when visualizing subnuclear pAkt localization by CLSM (Fig. 4g). Taken together, our data suggest that Pml can markedly increase effective concentrations of PP2a and its target, pAkt, in nuclear bodies, consistent with a nuclear pAkt clearing deficiency of *Pml^{-/-}* cells.

Characterization of the molecular pathways leading to cancer is a major step towards understanding and combating the disease²⁶. Here we have used mouse genetics to gather insights into AKT-driven tumorigenesis and established a mouse model for epithelial cancers triggered by *Pml* loss.

First, we have demonstrated the importance of *Pml* gene dose in prostate and colon carcinoma especially after *Pten* loss. For comparison, *Trp53*^{-/-} prostates never show neoplasia²⁷, and *Pten*^{+/-}*Trp53*^{-/-} prostates (ref. 27) or *Pten*^{+/-}*pRb*^{+/-} mice show no invasive prostate cancer (M. Niki and P.P.P., unpublished data). Second, *PML* loss highlights nuclear AKT function, a novel quality in *PTEN*-loss-driven tumorigenesis for which no model system exists so far. Colon, male prostate glands and female ovaries appear especially sensitive to increases in nuclear Akt and decreased Foxo3a levels. As we have shown that *p27^{kip1}* becomes a prostate and colon cancer inhibitor in conditions of *Pten* heterozygosity¹³, these results highlight the decisive role of FOXO3A function in human tumours with loss of one *PTEN* copy. Finally, we have identified a *Pten*-*Pml*-PP2a tumour-suppressive network for the inactivation of nuclear pAkt (see model, Supplementary Fig. S5d). Thus, PML regulates the activity of major opponents of AKT signalling in epithelia, which allows us to envision PML-stabilizing approaches for therapy of AKT-driven cancers.

METHODS

Mice

Pml^{-/-} (ref. 28) and *Pten*^{+/-} (ref. 7) mutants were crossed as described in Supplementary Information. The six cohort genotypes were: (1) *Pten*^{+/+} *Pml*^{+/+}; (2) *Pten*^{+/+} *Pml*^{+/-}; (3) *Pten*^{+/+} *Pml*^{-/-}; (4) *Pten*^{+/-} *Pml*^{+/+}; (5) *Pten*^{+/-} *Pml*^{+/-}; and, (6) *Pten*^{+/-} *Pml*^{-/-}.

MRI

For initial tumour assessment, mice of all genotypes were subjected to monthly MRI screening similar to the protocol described previously¹¹ (see also Supplementary Information).

Western blotting, immunoprecipitation and *in vitro* kinase assays

Tissue and cell lysates were prepared as previously described¹¹ and processed as outlined in Supplementary Information. *In vitro* kinase assays were done using a non-radioactive kinase kit (see Supplementary Information).

Cells, plasmids and immunofluorescence

Pten^{-/-} *Trp53*^{-/-} MEFs were prepared as described²⁷. Plasmids for FOXO3A and a FOXO3A mutant¹⁹ were gifts of M. Greenberg. The Flag-*PML* IV-derived plasmids were done as previously described²⁹. See Supplementary Information for further information.

IHC and quantifications

For IHC, tissues were fixed and embedded in paraffin according to standard procedures (see Supplementary Information) and determination of average prostate cell size was calculated as outlined in Supplementary Information.

Quantitative real time PCR

Tissue RNA was isolated using the Trizol method and quantitative real-time PCR performed as described³⁰. See Supplementary Information for all primer sets and detailed methods.

A detailed Methods section including antibodies used is available as online Supplementary Information.

Supplementary Material

Refer to Web version on PubMed Central for supplementary material.

Acknowledgements

We thank R. Bernardi, B. Carver, Z. Chen, S. Clohessy, T. Maeda and T. Yung for discussion, help with reagents and data analysis; W. Golden and M. S. Jiao for help with pathology analysis; and C. Le, M. Lupu and C. Matei for help with MR imaging. This work was supported by NIH grants to P.P.P. and P.P.S. as well as grants to J.A.K. and the Memorial Sloan-Kettering Cancer Center.

References

1. Luo J, Manning BD, Cantley LC. Targeting the PI3K–Akt pathway in human cancer: rationale and promise. *Cancer Cell* 2003;4:257–262. [PubMed: 14585353]
2. Brenkman AB, Burgering BM. FoxO3a eggs on fertility and aging. *Trends Mol Med* 2003;9:464–467. [PubMed: 14604822]
3. Salomoni P, Pandolfi PP. The role of PML in tumor suppression. *Cell* 2002;108:165–170. [PubMed: 11832207]
4. Gurrieri C, et al. Loss of the tumour suppressor PML in human cancers of multiple histologic origins. *J Natl Cancer Inst* 2004;96:269–279. [PubMed: 14970276]
5. Goel A, et al. Frequent inactivation of PTEN by promoter hypermethylation in microsatellite instability-high sporadic colorectal cancers. *Cancer Res* 2004;64:3014–3021. [PubMed: 15126336]
6. Porkka KP, Visakorpi T. Molecular mechanisms of prostate cancer. *Eur Urol* 2004;45:683–691. [PubMed: 15149739]
7. Di Cristofano A, Pesce B, Cordon-Cardo C, Pandolfi PP. Pten is essential for embryonic development and tumour suppression. *Nature Genet* 1998;19:348–355. [PubMed: 9697695]
8. Podsypanina K, et al. Mutation of Pten/Mmac1 in mice causes neoplasia in multiple organ systems. *Proc Natl Acad Sci USA* 1999;96:1563–1568. [PubMed: 9990064]
9. Suzuki A, et al. High cancer susceptibility and embryonic lethality associated with mutation of the PTEN tumor suppressor gene in mice. *Curr Biol* 1998;8:1169–1178. [PubMed: 9799734]
10. Di Cristofano A, et al. Impaired Fas response and autoimmunity in Pten^{+/-} mice. *Science* 1999;285:2122–2125. [PubMed: 10497129]
11. Trotman LC, et al. Pten dose dictates cancer progression in the prostate. *PLoS Biol* 2003;1:E59. [PubMed: 14691534]
12. Wang S, et al. Prostate-specific deletion of the murine *Pten* tumor suppressor gene leads to metastatic prostate cancer. *Cancer Cell* 2003;4:209–221. [PubMed: 14522255]
13. Di Cristofano A, De Acetis M, Koff A, Cordon-Cardo C, Pandolfi PP. Pten and p27KIP1 cooperate in prostate cancer tumor suppression in the mouse. *Nature Genet* 2001;27:222–224. [PubMed: 11175795]
14. Maehama T, Taylor GS, Dixon JE. PTEN and myotubularin: novel phosphoinositide phosphatases. *Annu Rev Biochem* 2001;70:247–279. [PubMed: 11395408]
15. Stambolic V, et al. Negative regulation of PKB/Akt-dependent cell survival by the tumor suppressor PTEN. *Cell* 1998;95:29–39. [PubMed: 9778245]
16. Sarbassov DD, Guertin DA, Ali SM, Sabatini DM. Phosphorylation and regulation of Akt/PKB by the rictor–mTOR complex. *Science* 2005;307:1098–1101. [PubMed: 15718470]
17. Brazil DP, Yang ZZ, Hemmings BA. Advances in protein kinase B signalling: AKTion on multiple fronts. *Trends Biochem Sci* 2004;29:233–242. [PubMed: 15130559]
18. Tran H, Brunet A, Griffith EC, Greenberg ME. The many forks in FOXO's road. *Sci STKE* 2003;RE5. [PubMed: 12621150]2003
19. Brunet A, et al. Akt promotes cell survival by phosphorylating and inhibiting a Forkhead transcription factor. *Cell* 1999;96:857–868. [PubMed: 10102273]
20. Castrillon DH, Miao L, Kollipara R, Horner JW, DePinho RA. Suppression of ovarian follicle activation in mice by the transcription factor Foxo3a. *Science* 2003;301:215–218. [PubMed: 12855809]

21. Hosaka T, et al. Disruption of forkhead transcription factor (FOXO) family members in mice reveals their functional diversification. *Proc Natl Acad Sci USA* 2004;101:2975–2980. [PubMed: 14978268]
22. Millward TA, Zolnierowicz S, Hemmings BA. Regulation of protein kinase cascades by protein phosphatase 2A. *Trends Biochem Sci* 1999;24:186–191. [PubMed: 10322434]
23. Gao T, Furnari F, Newton AC. PHLPP: a phosphatase that directly dephosphorylates Akt, promotes apoptosis, and suppresses tumor growth. *Mol Cell* 2005;18:13–24. [PubMed: 15808505]
24. Janssens V, Goris J, Van Hoof C. PP2A: the expected tumor suppressor. *Curr Opin Genet Dev* 2005;15:34–41. [PubMed: 15661531]
25. Li L, Ren CH, Tahir SA, Ren C, Thompson TC. Caveolin-1 maintains activated Akt in prostate cancer cells through scaffolding domain binding site interactions with and inhibition of serine/threonine protein phosphatases PP1 and PP2A. *Mol Cell Biol* 2003;23:9389–9404. [PubMed: 14645548]
26. Hanahan D, Weinberg RA. The hallmarks of cancer. *Cell* 2000;100:57–70. [PubMed: 10647931]
27. Chen Z, et al. Crucial role of p53-dependent cellular senescence in suppression of *Pten*-deficient tumorigenesis. *Nature* 2005;436:725–730. [PubMed: 16079851]
28. Wang ZG, et al. PML is essential for multiple apoptotic pathways. *Nature Genet* 1998;20:266–272. [PubMed: 9806545]
29. Guo A, et al. The function of PML in p53-dependent apoptosis. *Nature Cell Biol* 2000;2:730–736. [PubMed: 11025664]
30. Brunet A, et al. Stress-dependent regulation of FOXO transcription factors by the SIRT1 deacetylase. *Science* 2004;303:2011–2015. [PubMed: 14976264]

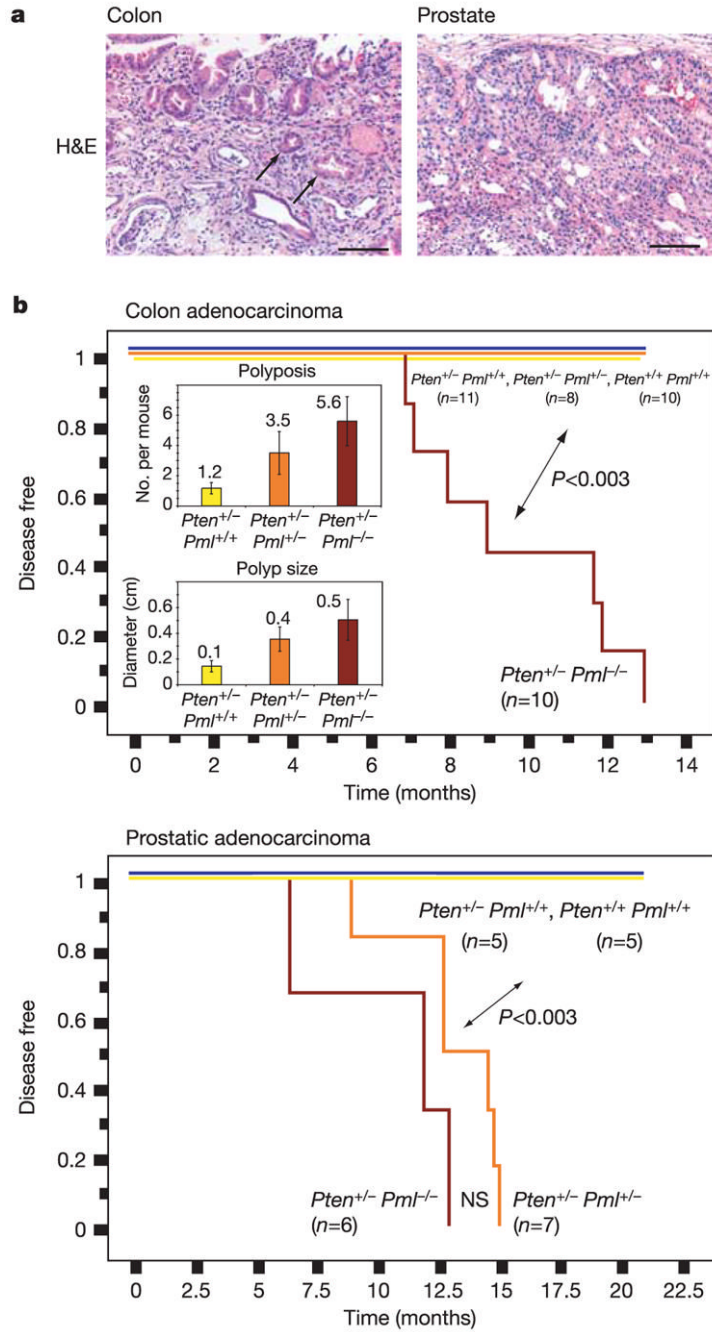


Figure 1. *Pml* status dictates carcinogenesis in *Pten*^{+/-} mice

a, Haematoxylin and eosin (H&E) analysis of colon and prostate tissue reveals invasive adenocarcinoma in *Pten*^{+/-} *Pml*^{-/-} mice. Arrows show invasive glands in colonic submucosa. Scale bars, 100µm. **b**, Kaplan–Meier plots for disease-free survival. Average polyps per mouse (top inset) and average polyp size (bottom inset) are shown. Error bars are s.d. (see also Methods).

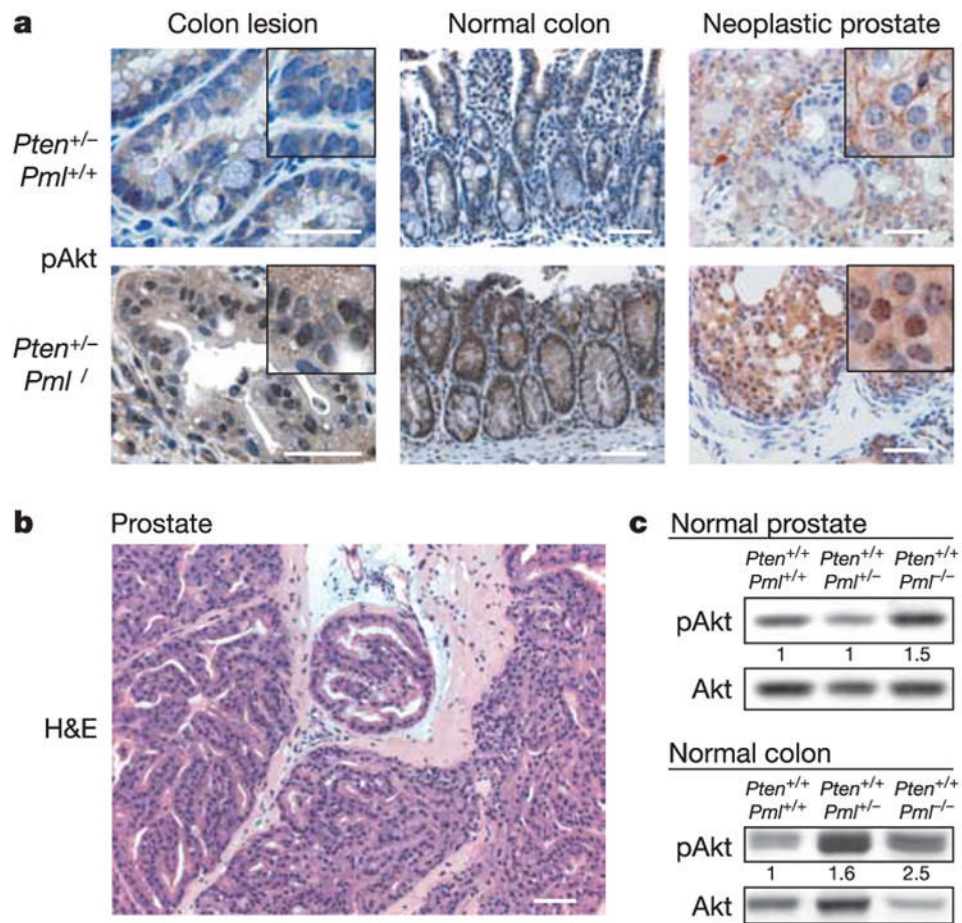


Figure 2. *Pml* loss leads to an increase in pAkt *in vivo*

a, IHC staining comparing pAkt levels and localization in *Pten*^{+/-} *Pml*^{+/+} and *Pten*^{+/-} *Pml*^{-/-} mice. **b**, Haematoxylin and eosin (H&E) staining of *Pml*^{-/-} prostate with high-grade prostatic intraepithelial neoplasia. Scale bars (**a**, **b**), 100µm. **c**, *Pml* status affects pAkt levels in pre-neoplastic *Pten*^{+/+} tissues.

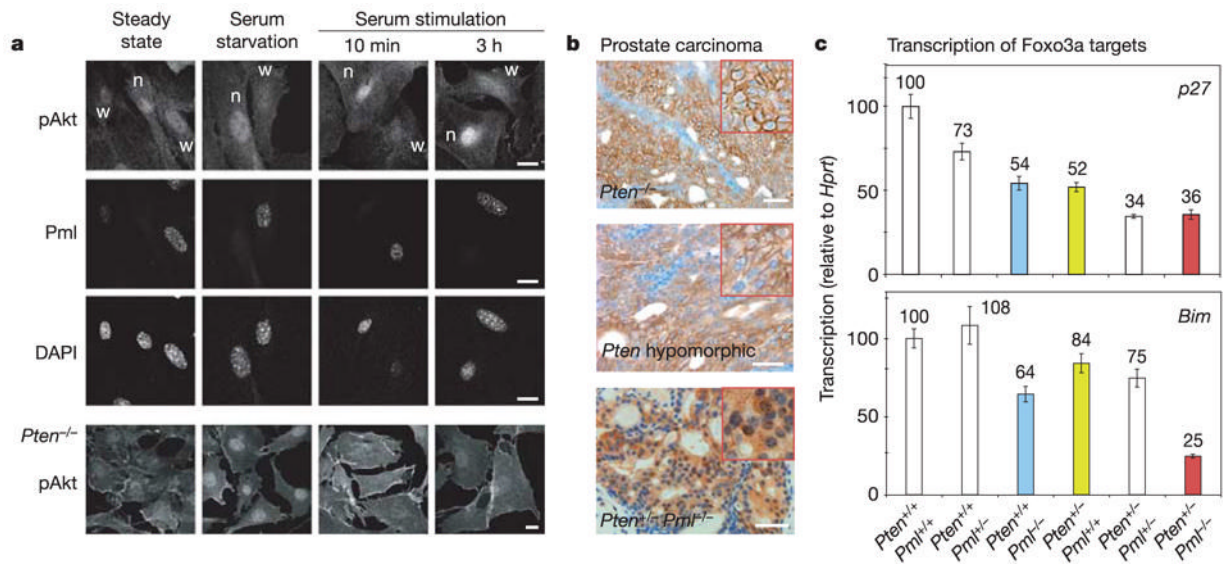


Figure 3. *Pml* deficiency leads to increased nuclear pAkt localization and function *in vitro* and *in vivo*

a, Immunofluorescence CLSM on primary littermate *Pml*^{+/+} (w) and *Pml*^{-/-} (n) MEFs seeded on the same coverslips. pAkt in *Pten*^{-/-} MEFs is shown for comparison. Scale bars, 10 μ m. **b**, pAkt in immunohistochemistry staining of prostate cancers from indicated mouse models. Scale bars, 50 μ m. **c**, Foxo3a activity measured by quantitative real-time PCR of prostates of the indicated genotypes. Error bars are s.d. of triplicates.

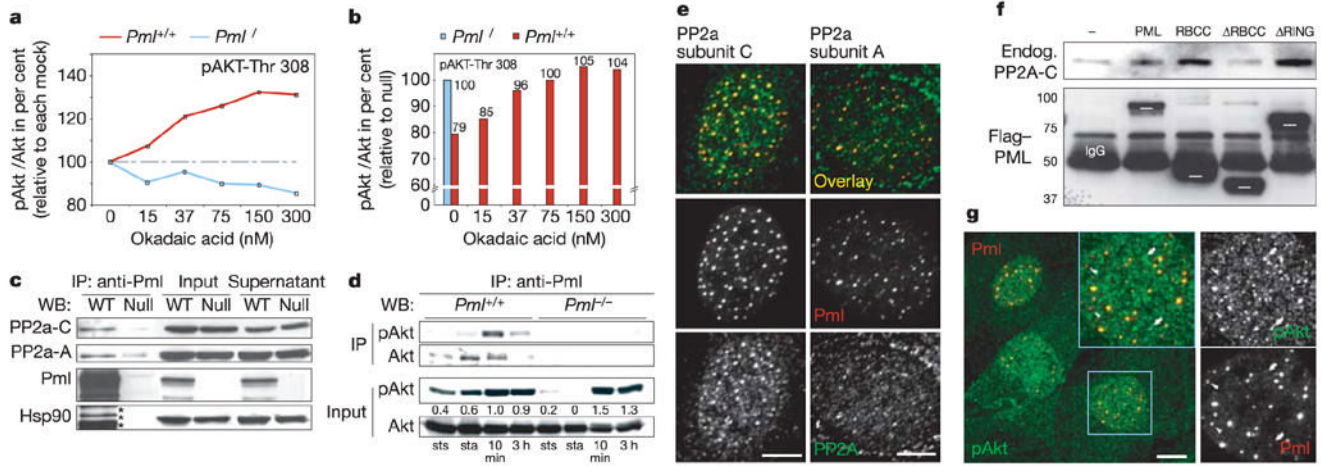


Figure 4. Pml affects PP2a activity towards pAkt

a, pAkt-Thr 308/Akt ratios after okadaic acid treatment of MEFs (relative to mock, see Methods). **b**, Ratios from **a** expressed relative to untreated *Pml*^{-/-} cells. Note the broken ordinate axis for clarity. **c**, Endogenous co-immunoprecipitation of PP2a with Pml in MEFs. Asterisks indicate leftover Pml staining, not Hsp90. **d**, Endogenous co-immunoprecipitation of Akt with Pml at steady state (sts), starvation (sta) and serum stimulation for times indicated. **e**, CLSM co-localization of endogenous Pml and PP2a in MEFs. Scale bars, 5 μ m. **f**, Anti-Flag co-immunoprecipitation of PP2a-C with Flag-tagged PML/PML mutants. White bars indicate PML/mutant migration. IgG, anti-Flag IgG heavy chains. Molecular weights are in kDa. **g**, CLSM co-localization of pAkt and Pml. Arrowheads indicate pAkt-deficient nuclear bodies and arrows indicate pAkt accumulation outside nuclear bodies. Scale bar, 10 μ m.